Supplement of Nonlin. Processes Geophys., 28, 311–328, 2021
https://doi.org/10.5194/npg-28-311-2021-supplement

Nonlinear Processes in Geophysics
Open Access
EGU

Supplement of

Comparing estimation techniques for temporal scaling in palaeoclimate time series

Raphaël Hébert et al.

Correspondence to: Raphaël Hébert (raphael.hebert@awi.de)

Contents

1 Block Average Results

Here we show the results of the analysis if block averaging was use to degrade the simulate “annual timeseries” instead of the filterind and sub-sampling method shown as the main result.

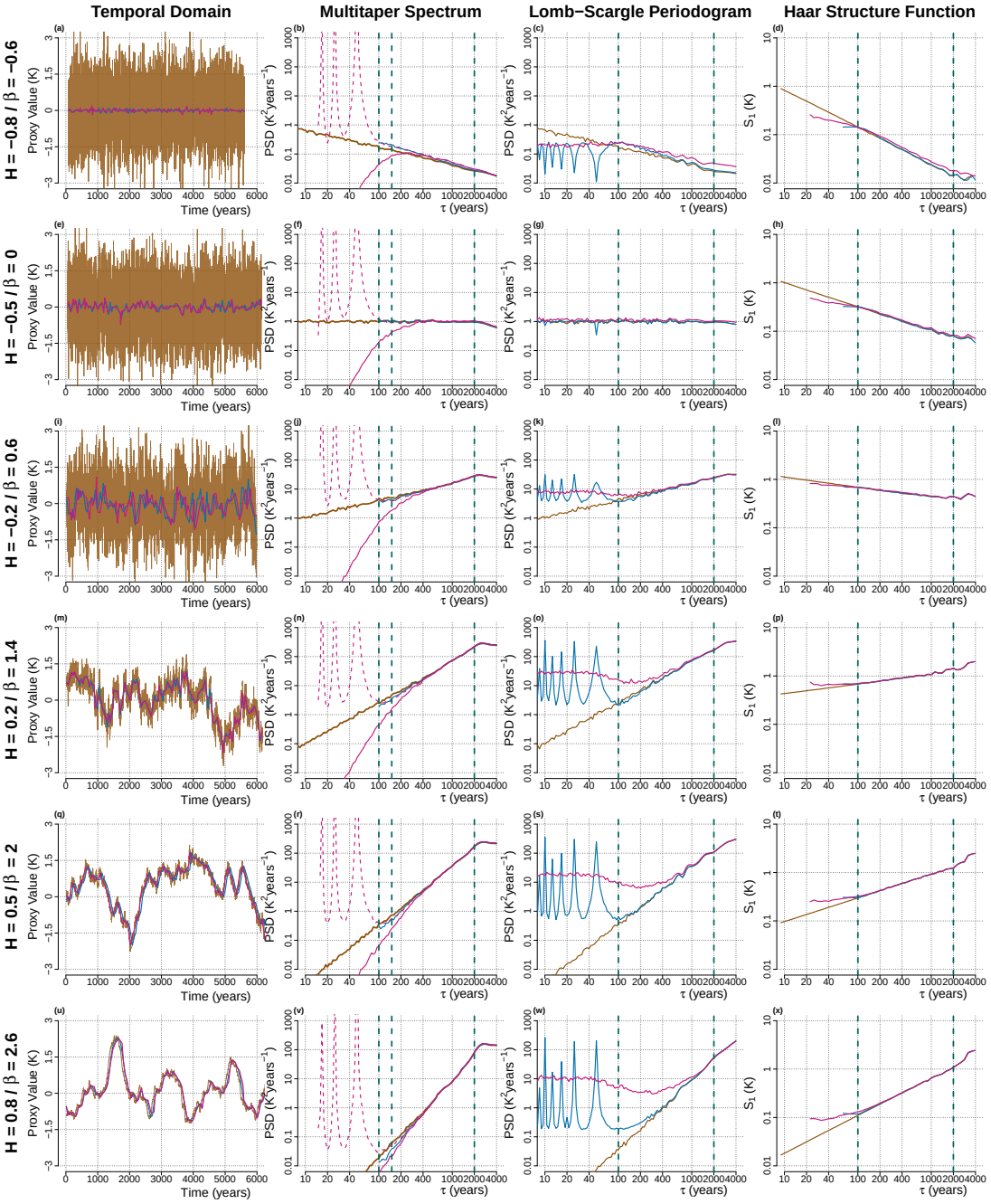

Figure S1. Same as Fig. 1, but using block averages to degrade the data rather than the lowpass filtering and subsampling. **(a,e,i,m,q,u)** Surrogate timeseries generated with a given H are shown at annual resolution (brown), degraded to a regular 50-year resolution (blue) and degraded to an irregular and random spacing drawn out of a gamma distribution with skewness $\nu = 1$ and mean 50 years. **(b,f,j,n,r,v)** Shown are the mean power spectra, estimated using the MTM, of 100 realizations of surrogate timeseries generated as in (a,e,i,m,q,u), respectively, and shown with the same colour scheme. The irregular case is also shown after dividing the power spectra by the expected $sinc^4$ bias due to interpolation (dashed pink). Also shown are the bounds for the fitting range considered later (vertical dashed blue): at the Nyquist frequency corresponding to 100 years, at 1.5 times the Nyquist frequency corresponding to 150 years and at one third the length of the timeseries at 2000 years. **(c,g,k,o,s,w)** Same as (b,f,j,n,r,v), respectively, but for the LSP instead of the MTM. **(d,h,l,p,t,x)**. Same as (b,f,j,n,r,v), respectively, but showing HSF instead of MTM power spectra.

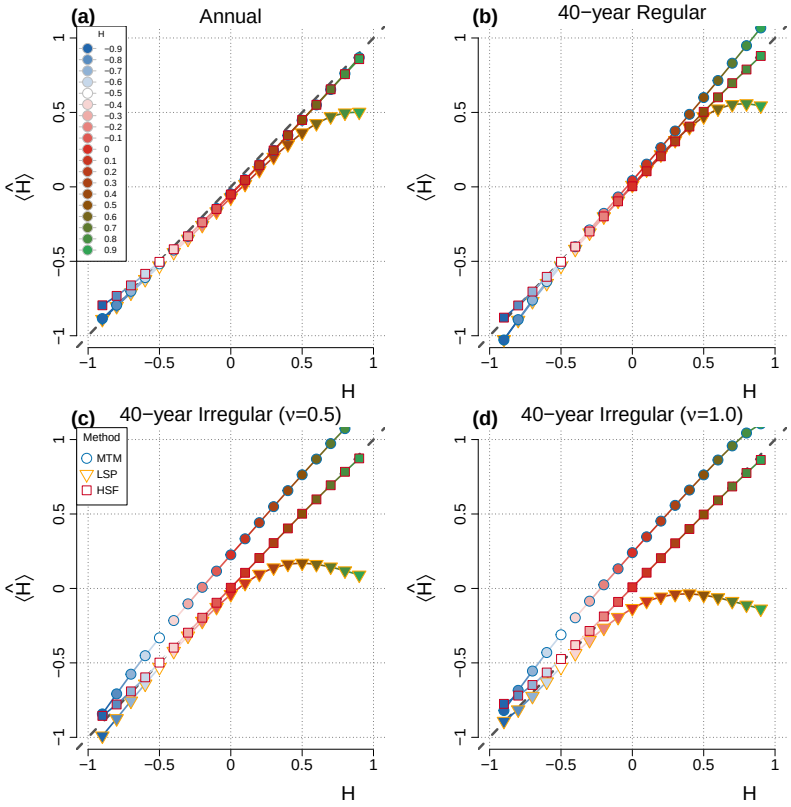

Figure S2. Same as Fig. 3, but using block averages to degrade the data rather than the lowpass filtering and subsampling. Deviations from the 1-to-1 line (dashed gray) correspond to the the bias B of the mean estimate $\langle \hat{H} \rangle$. The performance of the estimators is shown for regular and irregular surrogate data: **(a)** regular "annual data", i.e. it was directly simulated and not degraded after , **(b)** regular surrogate data degraded at regular 40-year interval, and irregular surrogate data with timesteps drawn from a gamma distribution with **(c)** skewness $\nu = 0.5$ or **(d)** skewness $\nu = 1$.

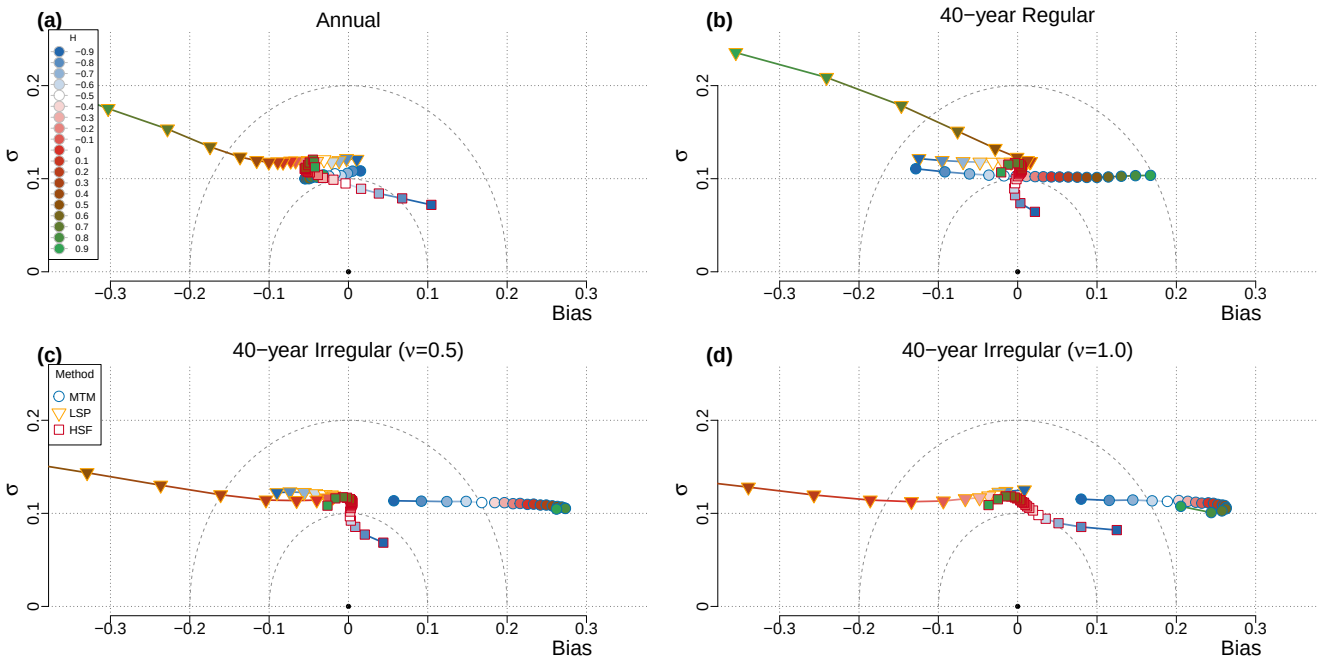

Figure S3. Same as Fig. 4, but using block averages to degrade the data rather than the lowpass filtering and subsampling. The performance of the estimators is shown for regular and irregular surrogate data: **(a)** regular "annual data", i.e. it was directly simulated and not degraded after , **(b)** regular surrogate data degraded at regular 40-year interval, and irregular surrogate data with timesteps drawn from a gamma distribution with **(c)** skewness $\nu = 0.5$ or **(d)** skewness $\nu = 1$.

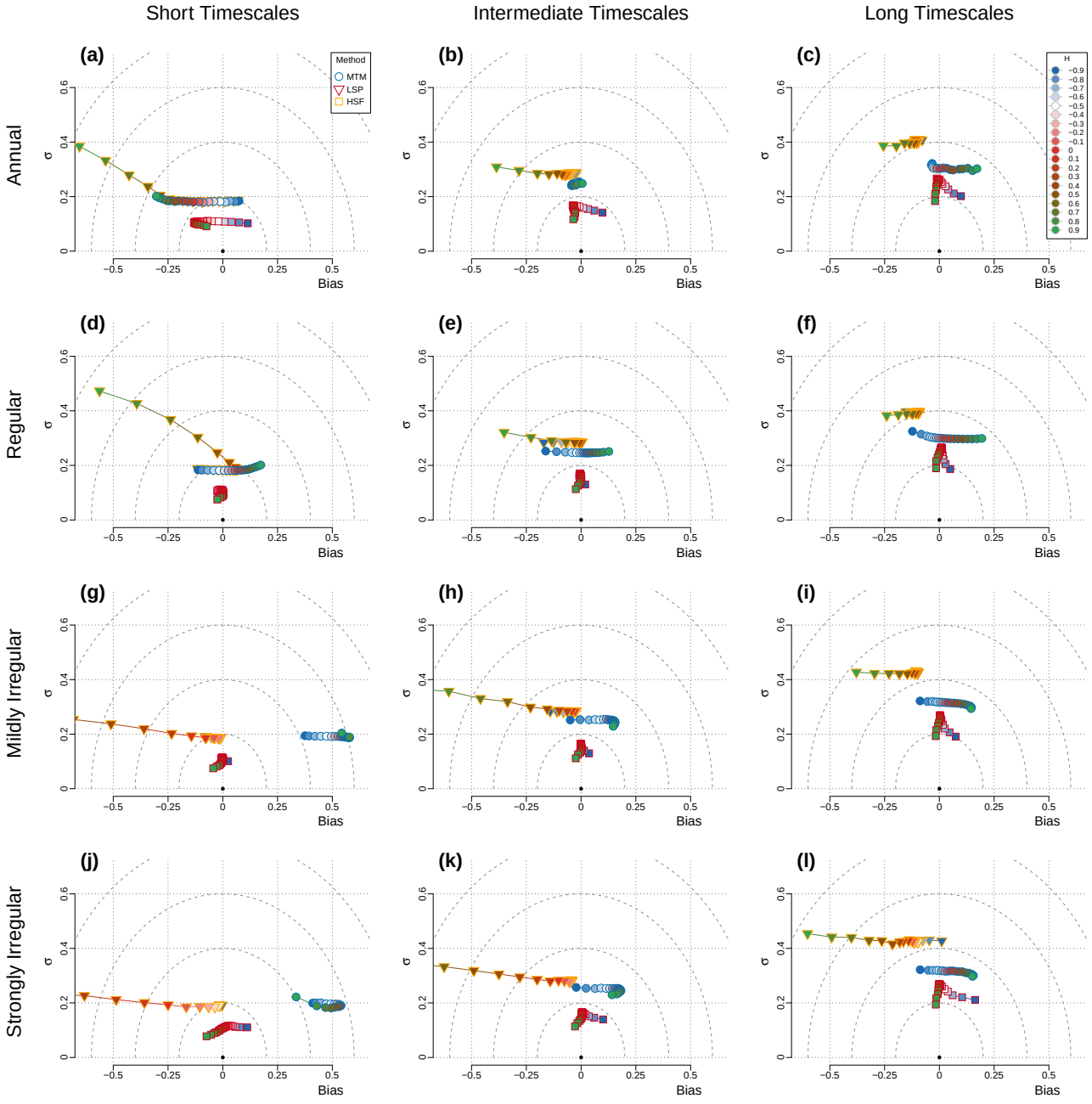

Figure S4. Same as Fig. 5, but using block averages to degrade the data rather than the lowpass filtering and subsampling. The timescale dependence of the bias and variance is evaluated for the three methods: MTM (circles), HSF (square), and LSP (triangles). The colors corresponds to the input H value for each simulation, ranging from -0.9 to 0.9. in increments of 0.1. The rows correspond to different types of surrogate series: **(a-c)** "annual data", **(d-f)** regular data , **(g-i)** mildy irregular data ($\nu = 0.5$), **(j-l)** strongly irregular data ($\nu = 1.0$); see section 2.2.1. The columns correspond to three different fitting ranges in terms of the mean resolution τ_μ, **(a,d,g,j)** the shorter timescales: 2-9.2 τ_μ, **(b,e,h,k)** the intermediate timescales: 4.3-19.9 τ_μ and **(c,f,i,l)** the longer timescales: 9.2-42.7 τ_μ

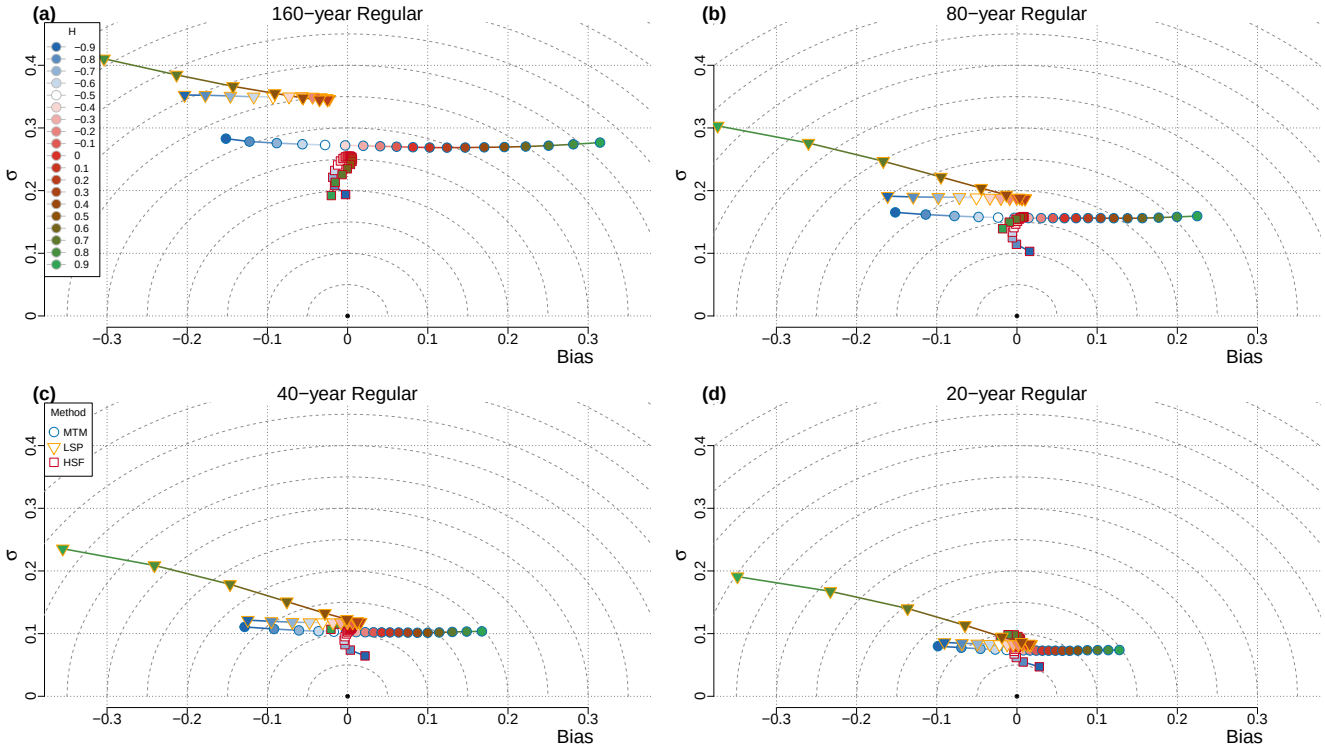

Figure S5. Same as Fig. 6, but using block averages to degrade the data rather than the lowpass filtering and subsampling. The performance of the estimators is shown for regular surrogate data of different resolutions: **(a)** 160 years , **(b)** 80 years, **(c)** 40 years and **(d)** 20 years. For each case, the series spanned 5120 years, and therefore each case contains 32, 64, 128 and 256 data points, respectively.

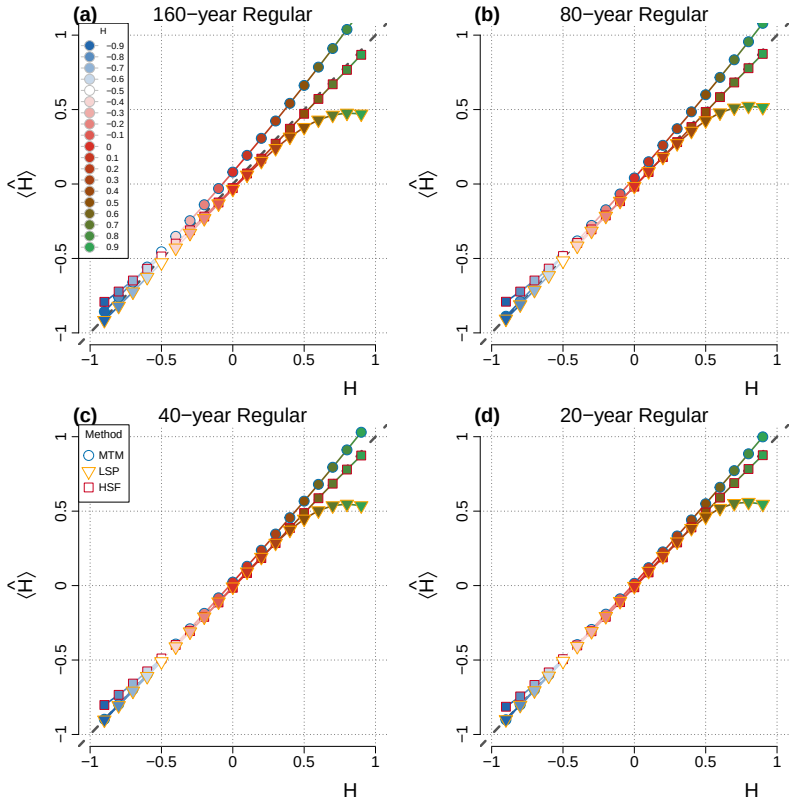

Figure S6. Same as Fig. 3, but for regular series of different resolutions. Deviations from the 1-to-1 line (dashed gray) correspond to the the bias B of the mean estimate $\langle \hat{H} \rangle$. The performance of the estimators is shown regular surrogate data of different resolutions: **(a)** 160 years , **(b)** 80 years, **(c)** 40 years and **(d)** 20 years. For each case, the series spanned 5120 years, and therefore each case contains 32, 64, 128 and 256 data points, respectively.

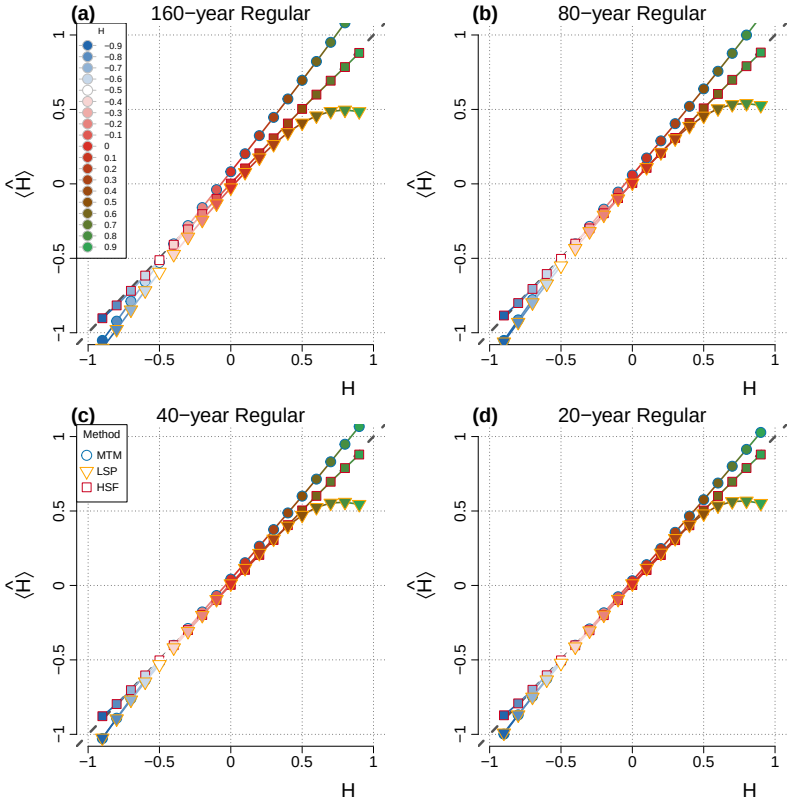

Figure S7. Same as Fig. S6, but using block averages to degrade the data rather than the lowpass filtering and subsampling.

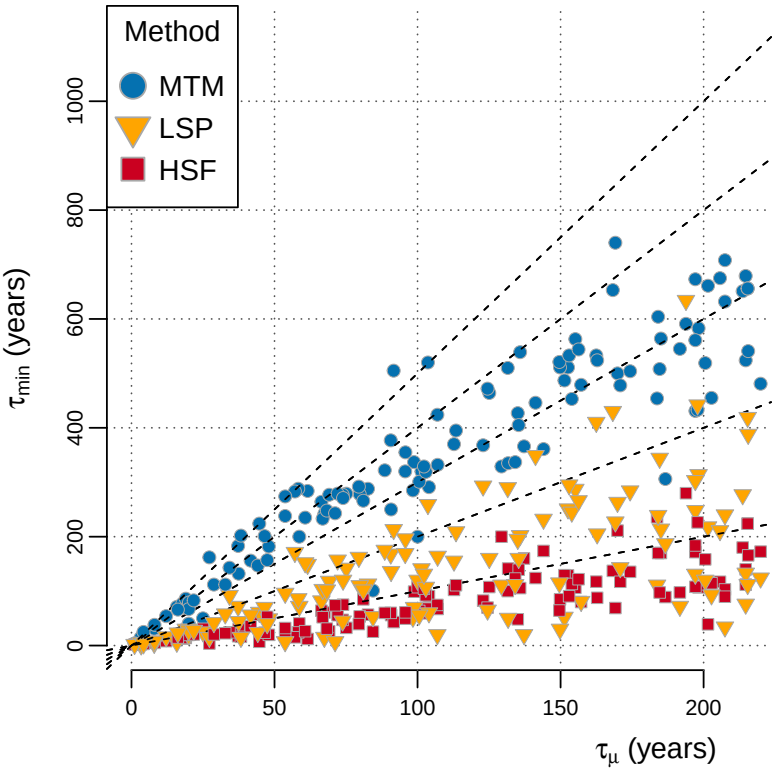

Figure S8. Same as Fig. 7, but with block averages rather than the lowpass filtering and subsampling. For each methods are shown the best minimum fitting timescales τ_{min} (minimizing the RMSE in H) as a function of the mean resolution τ_μ for ensembles of surrogate data generated with the same sampling scheme as the corresponding paleoclimate timeseries from the database.

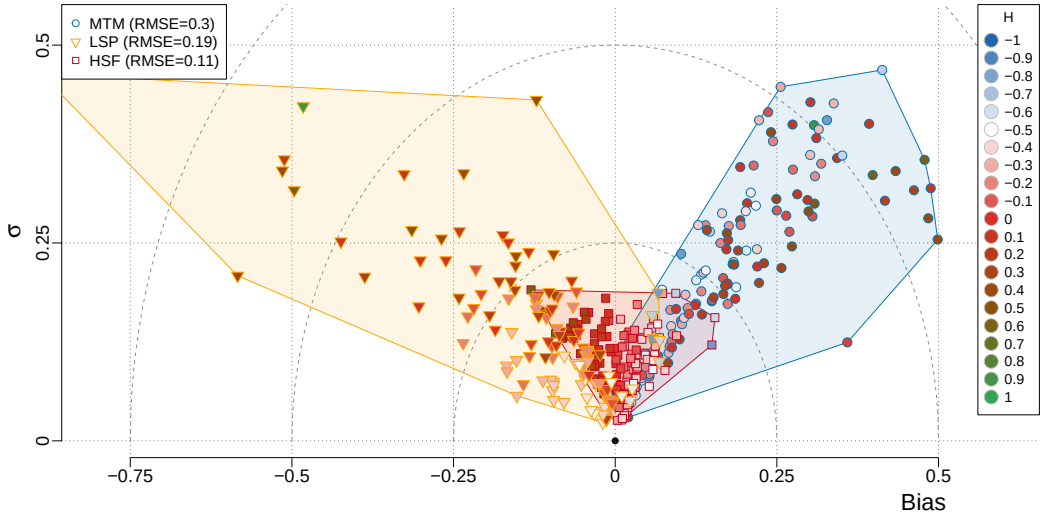

Figure S9. Same as Fig. 8, but with block averages rather than the lowpass filtering and subsampling. Bias-standard deviation diagram for the surrogate timeseries generated using timesteps from the paleoclimate database. The input H used to generate the timeseries is indicated by the colour inside the markers. The shaded polygons contain all the points for a given method (see legend for colours).

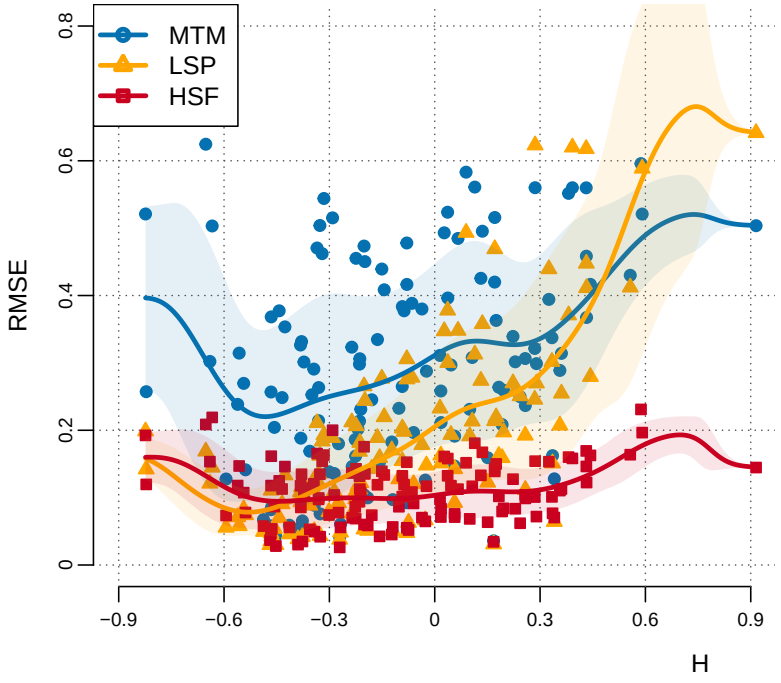

Figure S10. Same as Fig 9, but with block averages rather than the lowpass filtering and subsampling. Shown is the RMSE of the H estimates as a function of the input H for the surrogate timeseries based on the proxy database. The RMSE are given for the three estimation methods as a function of the H used to generate the surrogates. Also shown is a Gaussian smoothing of the points for each method (thick line) and the one standard deviation confidence interval (shaded).

2 First-Order Correction for the Effect of Interpolation

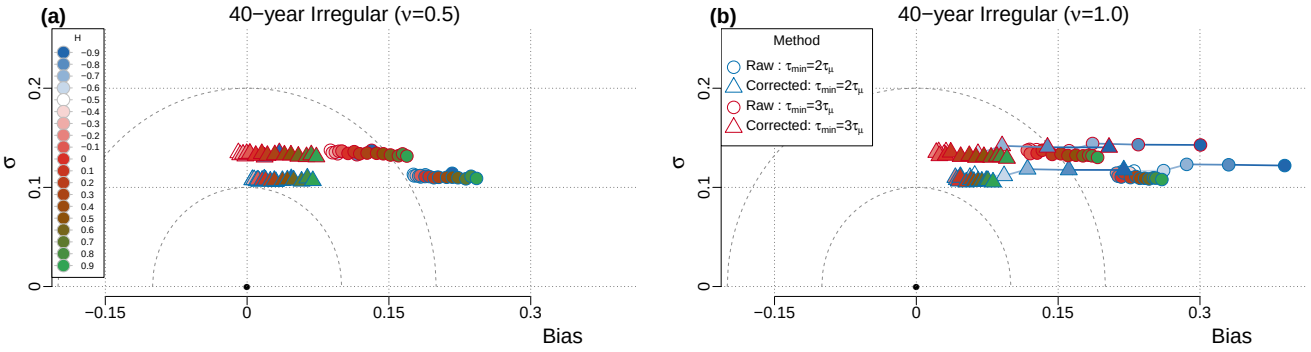

Figure S11. Bias-standard deviation diagram comparing the raw MTM estimates as given on Fig. 3 and a corrected version. In the corrected version, we attempted to account to first-order for the effect of the linear interpolation by dividing the estimated power spectra by a $sinc^4$ with timescale corresponding to the mean resolution of the irregular series. We show the results for two different minimum fitting timescales τ_{min}. This indicates that with such correction we could use the power spectral density estimates down to the Nyquist frequency (corresponding to twice the mean resolution τ_μ) with little bias instead of fitting from thrice the mean resolution as we did on Fig. 3.

3 Change in Bias and Standard Deviation

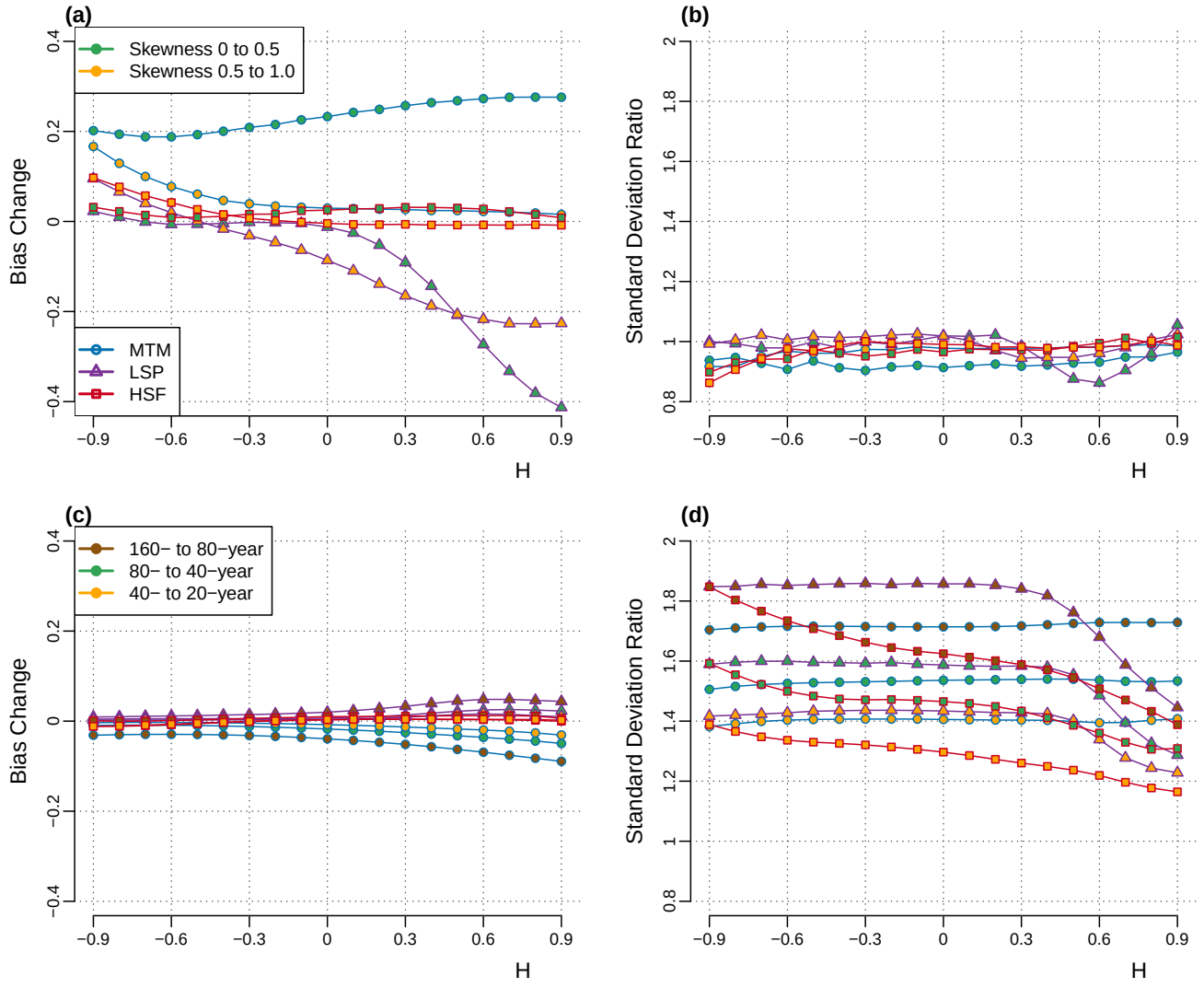

Figure S12. (a) The change in bias for the H estimates of each methods is shown when changing the skewness, from the regular to the mildly irregular case ($\nu = 0.5$, yellow), and the mildly irregular case to the strongly irregular case ($\nu = 1.0$, green). **(b)** Same as (a), but instead of the change in bias, it gives the factor by which the standard deviation of the H estimates decreases for each transition. **(c)**. Same as (a), but for changes in resolution, from 160- to 80- years (yellow), from 80- to 40- years (green) and from 40- to 20- years (brown). **(d)**. Same as (c), but instead of the change in bias, it gives the factor by which the standard deviation of the H estimates decreases for each of the resolution doublings. Overall, we notice that increase the skewness affects mostly the bias, whereas changing the resolution mostly affects the standard deviation of the estimates.